Chemical Science

ROYAL SOCIETY OF CHEMISTRY

EDGE ARTICLE

View Article Online
View Journal | View Issue

Cite this: *Chem. Sci.*, 2021, **12**, 9366

All publication charges for this article have been paid for by the Royal Society of Chemistry

Received 24th March 2021
Accepted 4th June 2021

DOI: 10.1039/d1sc01685g

rsc.li/chemical-science

High-yield and sustainable synthesis of quinoidal compounds assisted by keto–enol tautomerism†

Cheng Wang,[a] Tian Du,[a] Yunfeng Deng, *[a] Jiarong Yao,[b] Riqing Li,[b] Xuxia Zhao,[a] Yu Jiang,[c] Haipeng Wei,[c] Yanfeng Dang, *[b] Rongjin Li *[b] and Yanhou Geng [ac]

The classical synthesis of quinoids, which involves Takahashi coupling and subsequent oxidation, often gives only low to medium yields. Herein, we disclose the keto–enol-tautomerism-assisted spontaneous air oxidation of the coupling products to quinoids. This allows for the synthesis of various indandione-terminated quinoids in high isolated yields (85–95%). The origin of the high yield and the mechanism of the spontaneous air oxidation were ascertained by experiments and theoretical calculations. All the quinoidal compounds displayed unipolar n-type transport behavior, and single crystal field-effect transistors based on the micro-wires of a representative quinoid delivered an electron mobility of up to 0.53 $cm^2 V^{-1} s^{-1}$, showing the potential of this type of quinoid as an organic semiconductor.

Introduction

Quinoidal compounds have unique optical, electronic, and magnetic properties and therefore have potential applications in many fields.[1–7] In particular, the low-lying lowest unoccupied molecular orbital energy levels of these compounds make them ideal n-type semiconductors, which are crucial for the development of organic logic circuits and organic thermoelectrics.[4,8] In addition, they can be used as magnetic semiconductors for organic spintronics[5] and as singlet fission materials for photovoltaic devices due to their diradical character.[9–11]

Quinoidal compounds are typically synthesized by a two-step procedure involving (1) a Pd-catalyzed Takahashi coupling reaction to form an aromatic intermediate bearing a tertiary carbon center at each end of the aromatic moiety and (2) subsequent oxidation of the intermediate with a strong oxidant (Fig. 1a).[6,12,13] A myriad of quinoidal compounds have been synthesized *via* this method. However, the yields tend to be relatively low (<60% in most cases) even after optimization of the reaction conditions.[8,13–22] Particularly, an excess of an oxidant, such as aqueous Br_2 or 2,3-dichloro-5,6-dicyano-1,4-benzoquinone (DDQ), is often required for the oxidation,[8,13,15,17,20–22] which adds synthetic steps and produces stoichiometric wastes. In addition, when aqueous Br_2 is used as the oxidant, a bromination side-reaction that generates difficult-to-separate by-products may occur.[23] On the whole, there is still lack of a mild and an efficient method for the synthesis of quinoidal compounds. In the current paper, we report a protocol for the sustainable synthesis of indandione-terminated quinoidal compounds in high yields up to 95% by means of a highly efficient coupling reaction followed by spontaneous air oxidation of the resulting aromatic intermediate assisted by keto–enol tautomerism (Fig. 1b).

Results and discussion

Because diketopyrrolopyrrole (DPP)-based quinoidal compounds have been proved as good n-type

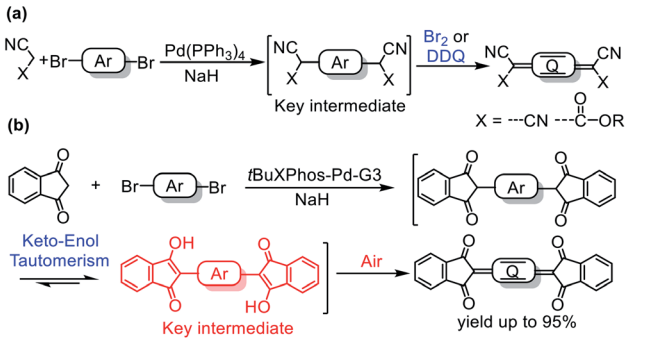

Fig. 1 Previously reported (a) and our (b) method for the synthesis of quinoidal compounds.

[a]*School of Materials Science and Engineering, Tianjin Key Laboratory of Molecular Optoelectronic Sciences, Tianjin University, Tianjin 300072, China. E-mail: yunfeng.deng@tju.edu.cn*

[b]*Tianjin Key Laboratory of Molecular Optoelectronic Sciences, Department of Chemistry, School of Science, Tianjin University, Tianjin 300072, China. E-mail: yanfeng.dang@tju.edu.cn; lirj@tju.edu.cn*

[c]*Joint School of National University of Singapore and Tianjin University, International Campus of Tianjin University, Binhai New City, Fuzhou 350207, China*

† Electronic supplementary information (ESI) available. CCDC 2062681. For ESI and crystallographic data in CIF or other electronic format see DOI: 10.1039/d1sc01685g

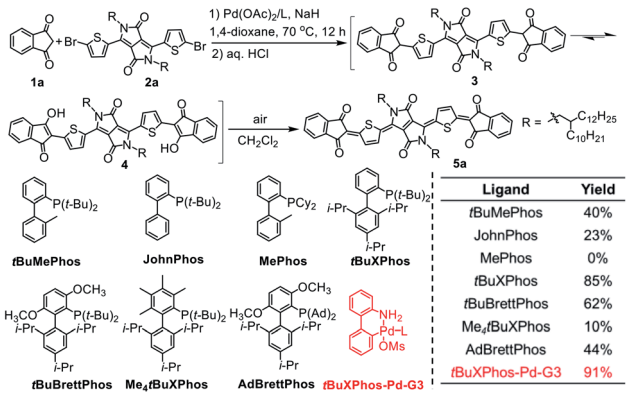

Ligand	Yield
*t*BuMePhos	40%
JohnPhos	23%
MePhos	0%
*t*BuXPhos	85%
*t*BuBrettPhos	62%
Me_4*t*BuXPhos	10%
AdBrettPhos	44%
*t*BuXPhos-Pd-G3	91%

Scheme 1 Ligand effects on the synthesis of quinoidal compound **5a**. Isolated yields are reported.

semiconductors[20,23,24] and indandione (**1a**) is a strongly electron-deficient moiety that can stabilize quinoidal structures and enhance intermolecular interactions,[12] we began our exploration of coupling conditions by using **1a** and bis(5-bromothiophen-2-yl)-substituted DPP (**2**) as substrates (Scheme 1). Unfortunately, the previously reported Takahashi coupling conditions[25,26] all failed to yield the desired intermediate. Inspired by a literature protocol for α-arylation of ketones,[27] we then attempted the coupling by using $Pd(OAc)_2$/*t*BuMePhos as the catalyst system and NaH as a base in 1,4-dioxane. Under these conditions, the desired quinoidal compound **5a** was obtained in 40% isolated yield. Surprisingly, we found that **5a** formed spontaneously after the coupling reaction was quenched by aqueous HCl and dichloromethane; that is, a separate oxidation step was unnecessary. This result suggests that the indandione-terminated aromatic intermediate was spontaneously converted to **5a** in air. In contrast, previous reports on the preparation of dicyanomethylene-substituted analogues all required a separate oxidation step with aqueous Br_2 as an oxidant.[20,24] Following this success, solvents, bases, Pd sources, and ligands were screened for the coupling reaction. It was found that the choice of the ligand was critical and that the moderately bulky ligand *t*BuXPhos gave the best results. With this ligand, **5a** was obtained in 85% yield, which is twice the yield obtained with *t*BuMePhos. This phenomenon can be explained by density functional theory (DFT) calculations (Fig. S2†), which revealed that reductive elimination was the rate-determining step of the coupling reaction. When *t*BuMePhos was replaced with *t*BuXPhos, the energy barrier for reductive elimination was significantly reduced from 28.0 to 17.8 kcal mol^{-1}, making the coupling more efficient. However, the use of bulkier ligands, such as *t*BuBrettPhos, Me_4*t*BuXPhos and AdBrettPhos, gave inferior results. We ascribed this phenomenon to the instability of the catalyst because very bulky ligands can readily dissociate from the Pd center.[28] In fact, Pd black formed when Me_4*t*BuXPhos was used as the ligand.

Buchwald precatalysts have proved to be highly active for a variety of Pd-catalyzed reactions,[29–31] so we next tested the third-generation Buchwald catalyst *t*BuXPhos-Pd-G3 as a single-component catalyst in our coupling reaction and found that **5a** could be obtained in a yield of 91%. Using this catalyst, we carried out reactions of several electron-deficient and electron-rich aromatic bromides (**2b–2g**). In all cases, the yields of the quinoidal compounds (**5b–5g**) were ≥85% (Table 1). Methyl substituted indandione was also applicable under the optimal conditions, giving the quinoidal compound (**5h**) in an isolated yield of 86%. Note that **5h** was obtained as the mixture of two isomers due to the asymmetry of the terminal groups. Again, all these quinoidal compounds formed spontaneously after the coupling reactions were quenched. These results demonstrate that our protocol has a wide substrate scope and that the structure of aromatic bromides has subtle effects on the coupling reaction and the subsequent spontaneous air oxidation. To the best of our knowledge, this is the first report on the synthesis of quinoidal compounds with isolated yields exceeding 90%.

Table 1 Substrate scope[a]

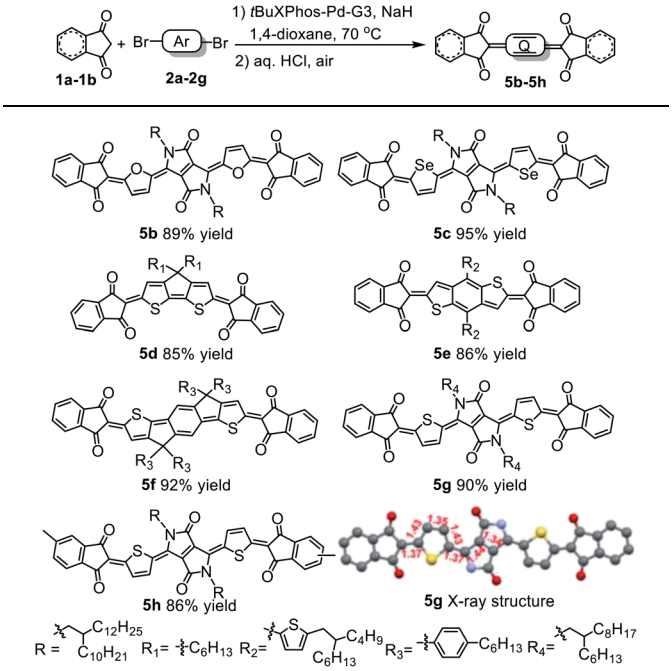

[a] Isolated yields are reported. For clarity, alkyl chains and hydrogen atoms are omitted in the X-ray structure of **5g**; bond lengths (Å) are indicated in red.

All the newly synthesized quinoidal compounds were characterized using ^1H and ^{13}C NMR spectroscopy and high-resolution matrix-assisted laser desorption ionization time-of-flight (HR MALDI-TOF) mass spectrometry. The structure of quinoidal compound **5g** was unambiguously confirmed by single-crystal X-ray diffraction analysis (Table 1). The central core of **5g** showed obvious bond length alternation, and the bond lengths between the terminal groups and the central core were close to the length of a typical $C(sp^2)$–$C(sp^2)$ double bond.

The high yields of the quinoidal compounds shown in Table 1 indicate that both the coupling step and the air oxidation step were highly efficient and that side reactions were negligible. To

obtain insights into the reaction mechanism, we first characterized the crude coupling product by NMR spectroscopy under argon (see the SI for details). As shown in Fig. S3a,† no resonance signals for the methine protons (CH) of terminal indandione moieties were observed in the ^{1}H NMR spectrum, suggesting that the coupling product existed in the enol form (**4**), rather than in the diketo form (**3**, see Scheme 1). This keto–enol tautomerism phenomenon was widely observed in the indandione-substituted aryl compounds.[32–34] The enolized structure can be further supported by the ^{13}C DEPT-135 NMR experiment, which did not show a positive signal at ~60 ppm attributable to the aliphatic CH of the terminal indandione moieties (Fig. S3b†).[34] All the resonance signals were consistent with the desired coupling product, and its molecular mass measured by MALDI-TOF spectrometry matched well with the calculated value (Fig. S4†). Note that the aromatic intermediate was not purified before measuring its NMR spectra. These results indicate that the coupling proceeded efficiently with negligible side reactions, and the aromatic intermediate **4** could be obtained in almost quantitative yield.

Next, we used UV-vis-NIR spectroscopy to monitor the oxidation of **4** in solution under bubbling air (Fig. 2a). The main absorption band in the spectrum of **4** gradually diminished over time, and a new absorption band appeared at 721 nm, which was assigned to **5a**. After 16 min, the absorption spectrum of the solution became the same as that of compound **5a**. Under UV light (254 nm), the oxidation time sharply decreased to 10 min (Fig. S5†). The above results suggest that compound **4** could be converted into **5a** completely in a short time by air oxidation. When the free-radical scavenger 2,6-di-*tert*-4-methylphenol (BHT, 2.0 equiv.) was added into the solution, the oxidation was markedly retarded (Fig. 2b), indicating that the oxidation involved radical species. Radical formation was also confirmed by electron paramagnetic resonance (EPR) spectroscopy. No signals were observed for the solution of **4** in argon or **5a** in air. However, a strong sharp signal was observed at a *g* value of 2.0039 for a solution of **4** under bubbling air (Fig. 2c). Interestingly, compound **4** can also be oxidized to **5a** by electrochemical oxidation, but the oxidation time is much longer than that of air oxidation. Besides, by-products were observed, as monitored by thin layer chromatography (Fig. S6 and S7†). Similar results were obtained after adding triethylamine and acetic acid (Fig. S6†), indicating that the effect of acid and base groups on the electrochemical oxidation of **4** is negligible.

We performed DFT calculations to clarify the oxidation mechanism. The calculated free-energy profiles for the air oxidation of **3** and **4** to give quinoid **5a** are shown in Fig. 3. In the oxidation of **3**, hydrogen abstraction by O_2 requires an energy barrier of 22.1 kcal mol^{-1} (*via* **TS1**), leading to **Int-1** and a peroxy radical (HOO$^{\bullet}$). Then, the peroxy radical acts as an oxidant to conduct the next hydrogen abstraction and generates the quinoidal product **5a**, which needs an energy barrier of 20.8 kcal mol^{-1} (*via* **TS2**). Because the oxidation occurs at room temperature (25 °C), the kinetic barriers for **TS1** and **TS2** are too high to explain the observed outcome of the reaction. In contrast, intermediate **3** can readily tautomerize to **4**, which can then undergo consecutive hydrogen abstraction processes (*via* **TS3** and **TS4**) by O_2 and the peroxy radical to afford **5a**. **TS3** and **TS4** have low energy barriers of 14.6 and 9.8 kcal mol^{-1}, respectively, which are readily achievable under the experimental conditions and are consistent with the observed spontaneous air oxidation of the coupling products to afford quinoids. Similar calculation results were observed for the formation of compound **5d** (Fig. S8†). Note that the only byproduct of air oxidation was H_2O_2, which can undergo disproportionation ($H_2O_2 \rightarrow H_2O + 1/2O_2$) to produce water,[35–37] making this a sustainable synthesis.[38–40] Taken together, our results demonstrate that the high yields of the quinoidal compounds were due to the quantitative formation of aromatic intermediates and their effective oxidation assisted by keto–enol tautomerism.

The solution UV-vis-NIR absorption spectra of **5a–5h** in toluene are shown in Fig. 4a and b, and the related data are summarized in Table S4.† The spectra of **5a**, **5g** and **5h** were nearly identical with the absorption maxima (λ_{max}) at 721 nm, suggesting that the change of alkyl chains and the introduction of methyl groups on the terminal benzene rings have minimal effect on the electronic structures of the molecules. In comparison with **5a**, the spectra of **5b** and **5c** were blue-shifted by 46 and 6 nm, respectively. A similar trend was also observed in other DPP-based quinoids.[41] The λ_{max} values were found to be red-shifted from 610 nm for **5d** to 661 nm for **5e** and then to 790 nm for **5f**. Going from solution to film state, the λ_{max} values of **5a**, **5b**, **5c**, **5d**, **5g** and **5h** were blue-shifted, while those of **5e**

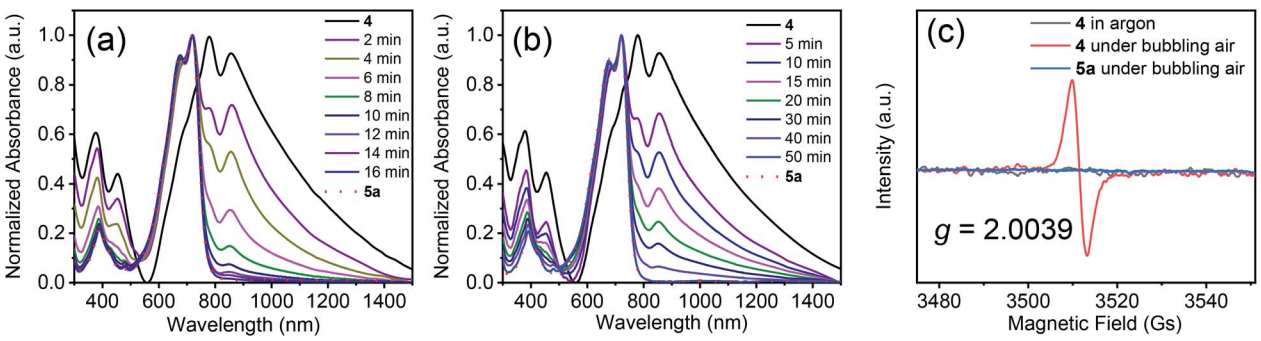

Fig. 2 Time dependence of UV-vis-NIR spectra of compound **4** in solution (CH_2Cl_2, 1×10^{-5} mol L^{-1}) without (a) and with (b) BHT (2.0 equiv.) under bubbling air. The EPR spectra of **4** in argon and under bubbling air and of **5a** under bubbling air (c).

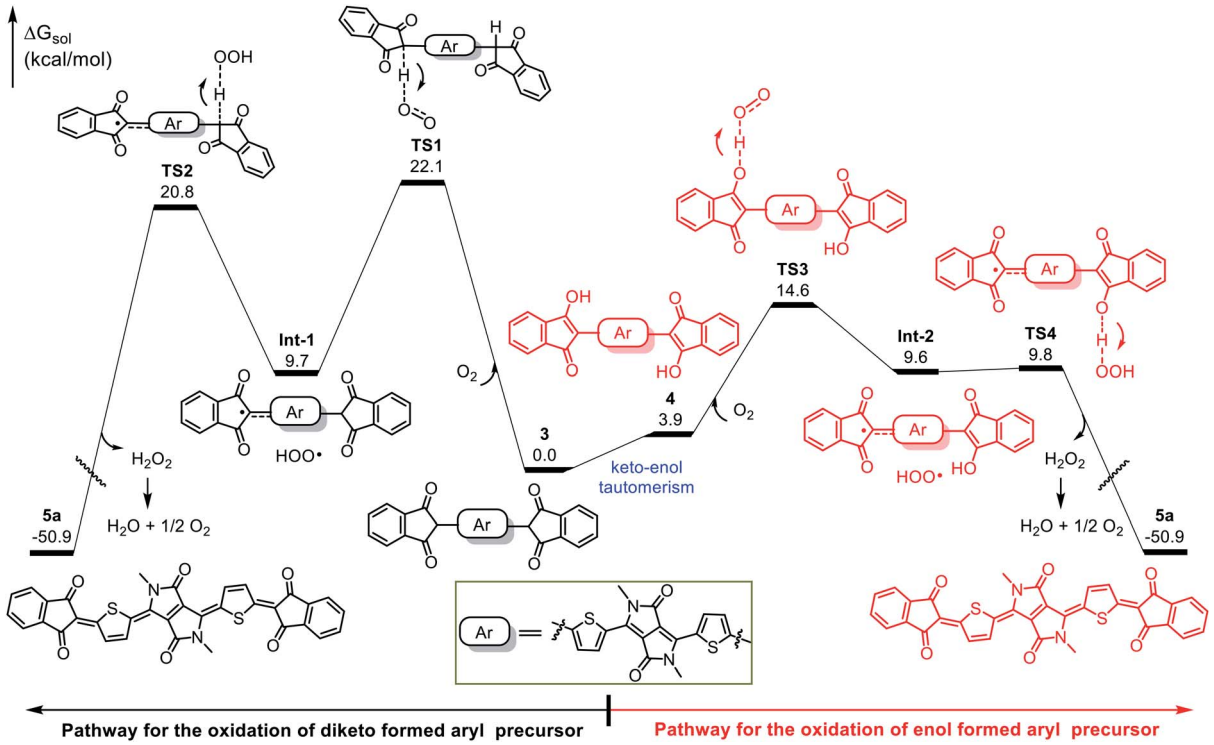

Fig. 3 Free-energy profiles for the oxidation of intermediates **3** and **4** to give quinoid **5a**.

and **5f** were significantly red-shifted (Fig. S10†). Particularly, **5e** showed a shift by 216 nm with the absorption onset extending to 1058 nm.

The electrochemical properties of **5a–5h** were characterized by solution cyclic voltammetry (Fig. S11†). The lowest unoccupied molecular orbital energy levels (E_{LUMO}) and the highest occupied molecular orbital energy levels (E_{HOMO}) were calculated based on the redox onset potentials, and the data are shown in Fig. 4c. All the quinoidal compounds exhibited reversible reduction couples, which is a typical characteristic of quinoids.[13,42–44] **5a** and **5g** had similar E_{HOMO} and E_{LUMO}. **5h** showed slightly higher E_{HOMO} and E_{LUMO} relative to **5a**, due to the electron-rich nature of the methyl group.[45] Changing the heterocycles from thiophene (**5a**) to furan (**5b**) led to high-lying E_{LUMO} and low-lying E_{HOMO}, while selenophene substitution (**5c**) only slightly elevated the E_{HOMO}. From **5d** to **5f**, the E_{LUMO} were gradually decreased, but the E_{HOMO} were gradually increased. Nevertheless, the E_{LUMO} of these compounds were below −4.0 eV, meeting the criterion for n-channel carrier transport in organic field-effect transistors (OFETs).[46]

Top-gate/bottom-contact (TGBC) OFETs were fabricated to investigate the charge transport properties of the quinoidal compounds. The active layers were fabricated by spin-coating from $CHCl_3$ solution. No transistor characteristics were observed for the devices based on **5d** and **5e**, whereas other compounds showed unipolar n-type transport behaviour. All the devices showed the best performance after annealing at 120 °C. Representative output and transfer curves of the optimal devices are shown in Fig. S12,† and the performance parameters are summarized in Table 2. The output and transfer curves showed negligible hysteresis between forward and reverse sweeps, indicating that there are only a few traps for electron

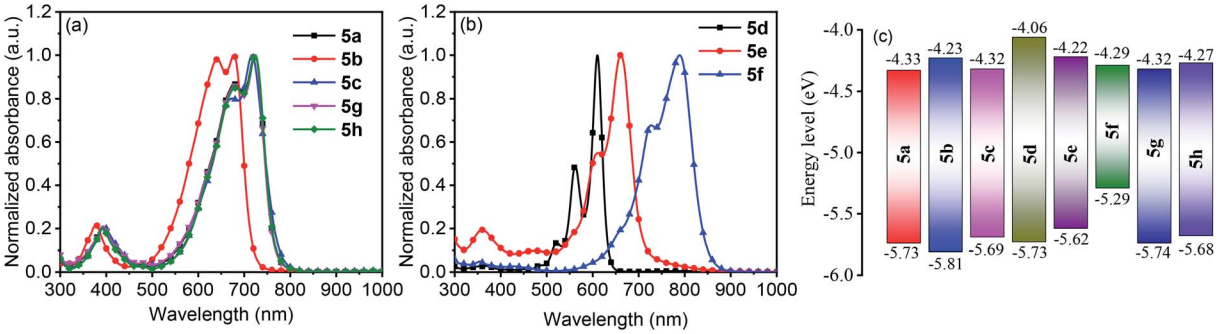

Fig. 4 Solution UV-vis-NIR absorption spectra of **5a–5h** in toluene (a and b) and HOMO/LUMO energy levels of **5a–5h** (c).

Table 2 TGBC OTFT device performances of the quinoidal compounds[a]

Compounds	$\mu_{e,max}$[b] ($cm^2\ V^{-1}\ s^{-1}$)	V_T[c] (V)	I_{on}/I_{off}[d]
5a	0.018 (0.015 ± 0.0017)	~12	~10^4
5b	0.016 (0.012 ± 0.0031)	~14	~10^4
5c	0.026 (0.022 ± 0.002961)	~15	~10^4
5f	0.21 (0.15 ± 0.039)	~13	~10^4
5g	0.007 (0.006 ± 0.0013)	~6	~10^4
5h	0.002 (0.0015 ± 0.0004)	~8	~10^4

[a] The devices were fabricated by spin-coating and annealed at 120 °C for 10 min in argon. [b] Mobilities were measured under ambient conditions. The values in parentheses are the average mobilities and the standard deviations from at least 5 devices. [c] Threshold voltage. [d] Current on/off ratio.

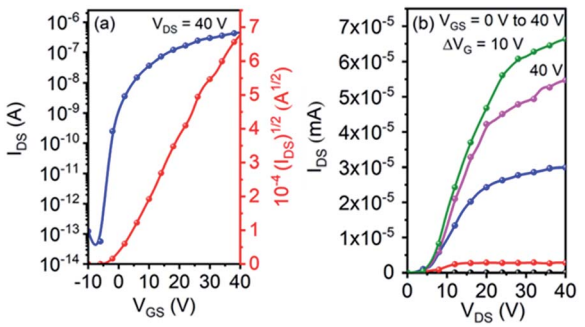

Fig. 5 Typical transfer (a) and output (b) characteristics of OFET based on the micro-wires of **5g**.

transport, largely attributed to their significantly lowered E_{LUMO}.[47,48] **5a** and **5b** delivered comparable performance with the electron mobility (μ_e) of ~0.018 $cm^2\ V^{-1}\ s^{-1}$. **5c** displayed a slightly high μ_e of 0.026 $cm^2\ V^{-1}\ s^{-1}$. In contrast, **5g** and **5h** showed inferior device performances with μ_e of 0.007 and 0.002 $cm^2\ V^{-1}\ s^{-1}$, respectively. The low mobility of **5h**, likely due to its poor solubility, prohibited the formation of a continuous thin film. Among these compounds, **5f** exhibited the best performance with a μ_e of up to 0.21 $cm^2\ V^{-1}\ s^{-1}$.

Single crystal OFET devices based on **5g** were fabricated because it could form micro-wires suitable for device application. Fig. 5 shows typical transfer and output characteristics of the devices measured under ambient conditions. An impressively high μ_e of up to 0.53 $cm^2\ V^{-1}\ s^{-1}$ was achieved. This value is remarkably higher than that of its thin-film counterpart. The device also exhibited a high current on/off ratio of ~10^7, along with a small threshold voltage of 3 V.

Conclusions

In conclusion, we herein reported a new approach to the high-yield and sustainable synthesis of quinoidal compounds. Specifically, highly efficient coupling of indandione and aryl bromides followed by keto–enol-tautomerism-assisted spontaneous air oxidation afforded indandione-terminated quinoidal compounds in isolated yields up to 95%. All the quinoidal compounds possessed low-lying LUMO energy levels of below −4.0 eV, which provided the n-type transport behaviour of these compounds. Single crystal OFET devices based on the micro-wires of **5g** displayed a high electron mobility of up to 0.53 $cm^2\ V^{-1}\ s^{-1}$. The present synthetic method may open a sustainable and fast way to access versatile quinoidal compounds and facilitate the evolution of new n-type semiconductors.

Data availability

CCDC 2046137 (**5g**) contains the supplementary crystallographic data for this paper. We include all extra related data in the supporting information.

Author contributions

The project was conceived and directed by Yunfeng Deng and Yanhou Geng. Cheng Wang, Tian Du and Xuxia Zhao conducted the experiments. Riqing Li and Yanfeng Dang conducted the DFT calculations. Jiarong Yao and Rongjin Li performed the single crystal OFET devices fabrication and characterization. Yu Jiang and Haipeng Wei involved the analysis of experimental results. All authors wrote the manuscript.

Conflicts of interest

There are no conflicts to declare.

Acknowledgements

This work was supported by the National Key R&D Program of "Strategic Advanced Electronic Materials" (no. 2016YFB0401100) of the Chinese Ministry of Science and Technology, National Natural Science Foundation of China (no. 52073209, 21774093) and Tianjin Natural Science Foundation (no. 19JCYBJC18100). Furthermore, Y. Deng would like to thank the Peiyang Scholar Program of Tianjin University for support.

Notes and references

1 J. Casado, R. Ponce Ortiz and J. T. López Navarrete, *Chem. Soc. Rev.*, 2012, **41**, 5672–5686.
2 C. K. Frederickson, B. D. Rose and M. M. Haley, *Acc. Chem. Res.*, 2017, **50**, 977–987.
3 Y. Sun, Y. Guo and Y. Liu, *Mater. Sci. Eng., R*, 2019, **136**, 13–26.
4 C. Zhang and X. Zhu, *Adv. Funct. Mater.*, 2020, **30**, 2000765.
5 X. Shi and C. Chi, *Top. Curr. Chem.*, 2017, **375**, 68.
6 K. Takimiya and K. Kawabata, *J. Synth. Org. Chem., Jpn.*, 2018, **76**, 1176–1184.
7 Y. Deng, B. Sun, Y. He, J. Quinn, C. Guo and Y. Li, *Angew. Chem., Int. Ed.*, 2016, **55**, 3459–3462.
8 K. Yang, X. Zhang, A. Harbuzaru, L. Wang, Y. Wang, C. Koh, H. Guo, Y. Shi, J. Chen, H. Sun, K. Feng, M. C. Ruiz Delgado, H. Y. Woo, R. P. Ortiz and X. Guo, *J. Am. Chem. Soc.*, 2020, **142**, 4329–4340.

9 H. Kim, B. Keller, R. Ho-Wu, N. Abeyasinghe, R. J. Vázquez, T. Goodson and P. M. Zimmerman, *J. Am. Chem. Soc.*, 2018, **140**, 7760–7763.
10 M. R. Momeni, *J. Chem. Theory Comput.*, 2016, **12**, 5067–5075.
11 S. Kawata, Y.-J. Pu, A. Saito, Y. Kurashige, T. Beppu, H. Katagiri, M. Hada and J. Kido, *Adv. Mater.*, 2016, **28**, 1585–1590.
12 T. Du, R. Gao, Y. Deng, C. Wang, Q. Zhou and Y. Geng, *Angew. Chem., Int. Ed.*, 2020, **59**, 221–225.
13 Y. Suzuki, E. Miyazaki and K. Takimiya, *J. Am. Chem. Soc.*, 2010, **132**, 10453–10466.
14 A. Velusamy, C.-H. Yu, S. N. Afraj, C.-C. Lin, W.-Y. Lo, C.-J. Yeh, Y.-W. Wu, H.-C. Hsieh, J. Chen, G.-H. Lee, S.-H. Tung, C.-L. Liu, M.-C. Chen and A. Facchetti, *Adv. Sci.*, 2021, **8**, 2002930.
15 D. Yuan, D. Huang, S. M. Rivero, A. Carreras, C. Zhang, Y. Zou, X. Jiao, C. R. McNeill, X. Zhu, C.-a. Di, D. Zhu, D. Casanova and J. Casado, *Chem*, 2019, **5**, 964–976.
16 D. Yuan, Y. Guo, Y. Zeng, Q. Fan, J. Wang, Y. Yi and X. Zhu, *Angew. Chem., Int. Ed.*, 2019, **58**, 4958–4962.
17 Y. Xiong, J. Tao, R. Wang, X. Qiao, X. Yang, D. Wang, H. Wu and H. Li, *Adv. Mater.*, 2016, **28**, 5949–5953.
18 L. Ren, D. Yuan, E. Gann, Y. Guo, L. Thomsen, C. R. McNeill, C.-a. Di, Y. Yi, X. Zhu and D. Zhu, *Chem. Mater.*, 2017, **29**, 4999–5008.
19 S. Wang, M. Wang, X. Zhang, X. Yang, Q. Huang, X. Qiao, H. Zhang, Q. Wu, Y. Xiong, J. Gao and H. Li, *Chem. Commun.*, 2014, **50**, 985–987.
20 Y. Qiao, Y. Guo, C. Yu, F. Zhang, W. Xu, Y. Liu and D. Zhu, *J. Am. Chem. Soc.*, 2012, **134**, 4084–4087.
21 J. Li, X. Qiao, Y. Xiong, H. Li and D. Zhu, *Chem. Mater.*, 2014, **26**, 5782–5788.
22 T. Mori, N. Yanai, I. Osaka and K. Takimiya, *Org. Lett.*, 2014, **16**, 1334–1337.
23 C. Wang, Y. Zang, Y. Qin, Q. Zhang, Y. Sun, C.-a. Di, W. Xu and D. Zhu, *Chem.–Eur. J.*, 2014, **20**, 13755–13761.
24 C. Wang, Y. Qin, Y. Sun, Y.-S. Guan, W. Xu and D. Zhu, *ACS Appl. Mater. Interfaces*, 2015, **7**, 15978–15987.
25 M. Uno, K. Seto and S. Takahashi, *J. Chem. Soc., Chem. Commun.*, 1984, **14**, 932–933.
26 T. Sakamoto, E. Katoh, Y. Kondo and H. Yamanaka, *Chem. Pharm. Bull.*, 1988, **36**, 1664–1668.
27 J. M. Fox, X. Huang, A. Chieffi and S. L. Buchwald, *J. Am. Chem. Soc.*, 2000, **122**, 1360–1370.
28 K. W. Anderson, T. Ikawa, R. E. Tundel and S. L. Buchwald, *J. Am. Chem. Soc.*, 2006, **128**, 10694–10695.
29 P. Ruiz-Castillo and S. L. Buchwald, *Chem. Rev.*, 2016, **116**, 12564–12649.
30 N. C. Bruno, M. T. Tudge and S. L. Buchwald, *Chem. Sci.*, 2013, **4**, 916–920.
31 A. Bruneau, M. Roche, M. Alami and S. Messaoudi, *ACS Catal.*, 2015, **5**, 1386–1396.
32 J. D. Pipkin and V. J. Stella, *J. Am. Chem. Soc.*, 1982, **104**, 6672–6680.
33 X. Shen, Y. Zheng and F. Wudl, *J. Mater. Chem. C*, 2016, **4**, 2427–2431.
34 A. Steigel, R. W. Veith and M. Braun, *Liebigs Ann. Chem.*, 1989, **1989**, 99–101.
35 A. J. Ingram, K. L. Walker, R. N. Zare and R. M. Waymouth, *J. Am. Chem. Soc.*, 2015, **137**, 13632–13646.
36 M. M. Konnick, B. A. Gandhi, I. A. Guzei and S. S. Stahl, *Angew. Chem., Int. Ed.*, 2006, **45**, 2904–2907.
37 Y. Dang, X. Deng, J. Guo, C. Song, W. Hu and Z.-X. Wang, *J. Am. Chem. Soc.*, 2016, **138**, 2712–2723.
38 A. N. Campbell and S. S. Stahl, *Acc. Chem. Res.*, 2012, **45**, 851–863.
39 K. M. Gligorich and M. S. Sigman, *Angew. Chem., Int. Ed.*, 2006, **45**, 6612–6615.
40 W. Wu and H. Jiang, *Acc. Chem. Res.*, 2012, **45**, 1736–1748.
41 W. Wang, L. Ge, G. Xue, F. Miao, P. Chen, H. Chen, Y. Lin, Y. Ni, J. Xiong, Y. Hu, J. Wu and Y. Zheng, *Chem. Commun.*, 2020, **56**, 1405–1408.
42 K. Yamamoto, S. Jinnai, T. Takehara, T. Suzuki and Y. Ie, *Org. Lett.*, 2020, **22**, 547–551.
43 K. Yamamoto, Y. Ie, M. Nitani, N. Tohnai, F. Kakiuchi, K. Zhang, W. Pisula, K. Asadi, P. W. M. Blom and Y. Aso, *J. Mater. Chem. C*, 2018, **6**, 7493–7500.
44 C. Wang, T. Du, Z. Liang, J. Zhu, J. Ren and Y. Deng, *J. Mater. Chem. C*, 2021, **9**, 2054–2062.
45 S. Li, L. Ye, W. Zhao, S. Zhang, S. Mukherjee, H. Ade and J. Hou, *Adv. Mater.*, 2016, **28**, 9423–9429.
46 Y. Sui, Y. Deng, T. Du, Y. Shi and Y. Geng, *Mater. Chem. Front.*, 2019, **3**, 1932–1951.
47 H. Sirringhaus, *Adv. Mater.*, 2014, **26**, 1319–1335.
48 T. Lei, X. Xia, J.-Y. Wang, C.-J. Liu and J. Pei, *J. Am. Chem. Soc.*, 2014, **136**, 2135–2141.